ELSEVIER

Journal of Power Sources 112 (2002) 222–230

JOURNAL OF POWER SOURCES

www.elsevier.com/locate/jpowsour

Electrochemical analysis for cycle performance and capacity fading of a lithium-ion battery cycled at elevated temperature

J. Shim, R. Kostecki, T. Richardson, X. Song, K.A. Striebel*

Environmental Energy Technologies Division, Lawrence Berkeley National Laboratory, Berkeley, CA 94720, USA

Received 23 June 2002; accepted 29 June 2002

Abstract

Laboratory-size $LiNi_{0.8}Co_{0.15}Al_{0.05}O_2$/graphite lithium-ion pouch cells were cycled over 100% DOD at room temperature and 60 °C in order to investigate high-temperature degradation mechanisms of this important technology. Capacity fade for the cell was correlated with that for the individual components, using electrochemical analysis of the electrodes and other diagnostic techniques. The high-temperature cell lost 65% of its initial capacity after 140 cycles at 60 °C compared to only a 4% loss for the cell cycled at room temperature. Cell ohmic impedance increased significantly with a elevated temperature cycling, resulting in some of loss of capacity at the *C*/2 rate. However, as determined with slow rate testing of the individual electrodes, the anode retained most of its original capacity, while the cathode lost 65%, even when cycled with a fresh source of lithium. Diagnostic evaluation of cell components including X-ray diffraction (XRD), Raman, CSAFM and suggest capacity loss occurs primarily due to a rise in the impedance of the cathode, especially at the end-of-charge. The impedance rise may be caused in part by a loss of the conductive carbon at the surface of the cathode and/or by an organic film on the surface of the cathode that becomes non-ionically conductive at low lithium content.
Published by Elsevier Science B.V.

Keywords: Li-ion battery; Cycle-life; $LiNi_{0.8}Co_{0.15}Al_{0.05}O_2$

1. Introduction

Extensive research on the rechargeable lithium-ion battery has been carried out with the goal of the development of electric vehicles [1–3]. While cells for electric vehicles will be operated at ambient temperature, lithium-ion cells cycled with currents greater than 2*C* can experience an internal temperature of more than 38 °C [4]. When a 100 Ah class lithium-ion battery module is tested for electric vehicle, the temperature difference between charging and discharging inside the module was 8 °C [5]. In both of the cases, they monitored temperature on the surface of the cell case, not inside of the cell or on the surface of the electrode. The temperature on the surface of the electrode may be significantly higher. This may be exacerbated by high-pulse cycling as required for high-power cells in the hybrid electric vehicle application.

Limited studies of lithium-ion cells cycled at temperatures over 50 °C have been reported. As part of the advanced technology development (ATD) program at the Lawrence Berkeley National Laboratory (LBNL), for the development of a high-power battery for the hybrid electric vehicle, researchers have developed several diagnostic techniques for the determination of capacity and power fade mechanisms in 18650-size lithium-ion cells during life-cycle pulse testing at temperatures up to 70 °C [6]. The high-temperature studies were used primarily as an accelerated aging technique. Cells were pulse-tested with a high-power profile but only with a very narrow range of variation of state of charge, as described in the PNGV test manual [7]. The capacity of these cells was found to be quite stable. The large increases in cell impedance with both cycling and aging at elevated temperature were attributed to non-uniformity of the SEI layer, electrolyte decomposition, current collector corrosion and/or nanocrystalline deposits and phase segregation in the cathode.

In a related project, we are focusing on the development of a high-energy battery for an all-electric vehicle and our group is studying the cycling performance and power fade mechanism of various battery chemistries during constant current cycling over 100% of the cell capacity [8]. Part of our goal is to elucidate differences in the capacity and power fade mechanisms that occur as a result of elevated

* Corresponding author. Tel.: +1-510-486-4385; fax: +1-510-486-7303.
E-mail address: kastriebel@lbl.gov (K.A. Striebel).

0378-7753/02/$ – see front matter. Published by Elsevier Science B.V.
PII: S0378-7753(02)00363-4

temperature, aging, depth of discharge and voltage range. In this work, we report on the performance of cells, containing electrodes designed for high-power operation with the latest ATD cell chemistry, cycled at 100% DOD at 25 and 60 °C. In order to aid in identification of failure mechanisms, several diagnostic techniques were used to analyze cell components.

2. Experimental

2.1. Cell construction

Cathodes and anodes for testing were supplied by Quallion Corp. (Sylmar, CA). The cathode consists of 84% $LiNi_{0.8}Co_{0.15}Al_{0.05}O_2$ (Fuji CA1505), 4% carbon black (Chevron), 4% SFG-6 (Timical) and 8% PVdF (Kureha) on aluminum foil (thickness 30 μm). The thickness and loading on the cathode are 70 μm and 9.1 mg/cm^2, respectively. The anode consists of 92% MAG-10 graphite (Hitachi Chemical) and 8% PVdF (Kureha) on copper foil (thickness 18 μm). The total thickness and loading of anode are 70 μm and 5.0 mg/cm^2, respectively.

Pouch cells were constructed from 12 cm^2 single-side coated anodes and cathodes sealed in an aluminum-foil laminated polymer film. The anode and cathode have metal (Ni or Al) tabs attached by ultrasonic welding for electrical connection. The anode was wrapped in Celgard 2500 separator to protect it against shorting. Cells were vacuum-filled with LP40 electrolyte (EM Science) with a composition of 1 M $LiPF_6$ in EC/DEC. This chemistry is identical to that used in the ATD Gen 2 [9], except for the electrolyte.

2.2. Cell cycling

After assembly, cells were subjected to a formation cycle by charging and then discharging at a low rate (*C*/25). This protocol should form a smooth SEI layer on the surface of the anode and slow gas evolution by the decomposition of the electrolyte [10,11]. After formation, cells were charged at the chosen current to a voltage limit of 4.1 V, followed by holding at 4.1 V until the current dropped below *C*/20 or for a maximum of 2 h. The discharging was constant current to a voltage of 3.0 V. This protocol is considered to be 100% DOD. All cycling was carried out with a Maccor Battery Cycler. Impedance studies of the cells before and after cycling were carried out with the Solartron 1260 FRA and a potentiostat.

2.3. Electrochemical diagnostics

After cycling at 60 °C, the pouch cell was disassembled in an He-atmosphere glovebox and each component was washed in dimethyl carbonate for 24 h and dried at room temperature in vacuum. Pieces of 1 cm^2 were punched from the 12 cm^2 electrodes and assembled against Li metal in Swagelok cells with fresh LP4O electrolyte. Slow-sweep electrochemical analysis of the individual electrodes was carried out at *C*/25 with the VMP Potentiostat/Galvanostat from BioLogic.

2.4. Physical diagnostics

A series of diagnostic studies were carried out with the remaining pieces of washed anode and/or cathode. X-ray diffraction (XRD) was carried out on the cathode with a Siemens D-5000 machine. A partially charged ($x = 0.5$) reference sample was prepared by chemical lithiation. For TEM measurements, a part of the anode was dispersed in EMC, ground lightly and then some of the particles were collected on a copper grid. Then it was sealed in a small bottle for transportation. A Philips CM200/FEG (field emission gun) TEM at the National Center for Electron Microscopy (NSEM) at LBNL was used to examine the electrode sample.

An integrated Raman microscope system ''Labram'' made by ISA Groupe Horiba was used to analyze the structure and composition of both the anode and the $LiNi_{0.8}Co_{0.15}Al_{0.05}O_2$ cathodes. The excitation wavelength was supplied by an internal He–Ne (632 nm) 10 mW laser. The power of the laser beam was adjusted to 0.1 mW with neutral filters of various optical densities. The size of the laser beam at the sample was ∼1.6 mm.

Current-sensing atomic force microscopy (CSAFM) was used to image the surface of the $LiNi_{0.8}Co_{0.15}Al_{0.05}O_2$ cathodes under a controlled N_2 atmosphere. The microscope consisted of a molecular imaging (MI) scanning probe microscope coupled with a Park Scientific Instruments (PSI) AutoProbe Electronic Module. The Si atomic force microscope (AFM) tips were coated with a thin conductive layer of W_2C. All CSAFM experiments were performed in constant-force mode with controlled oxide-tip voltage difference. A single scan of the tip over the cathode surface simultaneously produced two images: a topographic image and a conductance image; the latter represents oxide-tip current variations during scanning at a given oxide-tip voltage difference.

3. Results

3.1. Cycling capacity at elevated temperature

After room temperature formation, cells were cycled at 25 and 60 °C for 10 cycles at each of four different rates: *C*/5, *C*/2, *C* and 2*C*, corresponding to current densities from 0.23 to 2.33 mA/cm^2. The dependence of discharge capacity on cycling rate is summarized in Fig. 1. The capacity decreases only slightly (10%) as the rate is increased by a factor of 10 for these well-designed high-power electrodes. This is similar to the behavior observed with larger (100 and 900 mAh) cells made by Quallion with this same chemistry [12]. The variation of capacity at high rate will be determined by

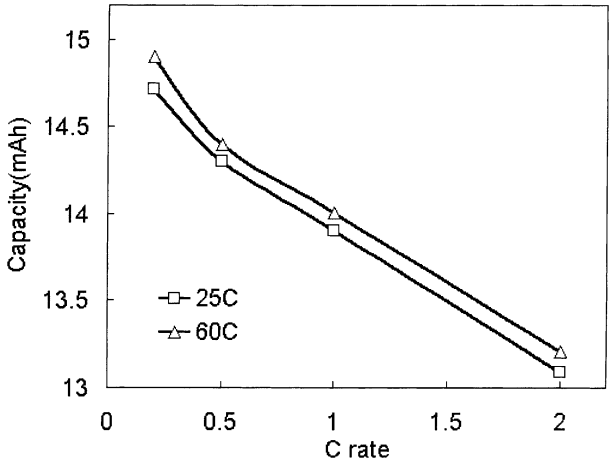

Fig. 1. Capacity of pouch cell at different *C* rates.

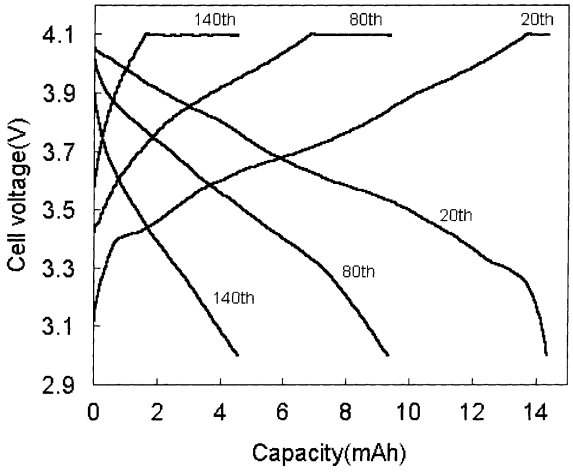

Fig. 3. Voltage profiles for pouch cell cycled at 60 °C, *C*/2 rate (6.0 mA).

several processes in the cell, including electrical conductivity within the electrode, diffusion and migration processes in the electrolyte. Although the conductivity of the electrolyte should almost double with this temperature rise, this did not significantly affect the rate behavior of the entire cell. This suggests that the behavior is more sensitive to the nature of the electrodes.

Following the variable rate characterization, cycling was continued at a rate of *C*/2 for an additional 100 cycles. Fig. 2 shows discharge capacity for the two cells including both the variable and constant rate cycling periods. The cell cycled at 25 °C shows a constant capacity at the *C*/2 rate loosing less than 4% of its original capacity after 140 cycles. However, the cell cycled at 60 °C shows rapid capacity fade with only 80 and 35% of the original capacity remaining in cycles 70 and 140, respectively. The remainder of the discussion will be geared towards understanding the mechanisms responsible for this capacity fade.

Voltage profiles from cycles 20, 80 and 140 for the cell cycled at 60 °C are compared in Fig. 3. The capacity for charging and discharging significantly decreased at elevated temperature. At the 20th cycle, there are many steps for lithium intercalation/deintercalation, but after 140 cycles the steps have almost completely disappeared and voltage increases and decreases sharply. During cycling, the required time for constant voltage charging increased continuously. These are characteristic of an increase in cell impedance.

After cycling, full-spectrum impedance measurements were made on the cells at a series of temperatures. Fig. 4 shows the room-temperature Nyquist plots for a fresh cell and 60 °C-cycled cell at 100% SOC. The impedance of the high-frequency process changes only slightly with cycling at 60 °C. However, the size of the low-frequency semi-circle greatly increased. It has been proposed that the high- and low-frequency processes corresponding to these semi-circles can be assigned to the interfacial resistances in the anode and cathode, respectively [13]. These results would then suggest that the increased cell impedance stems primarily from the

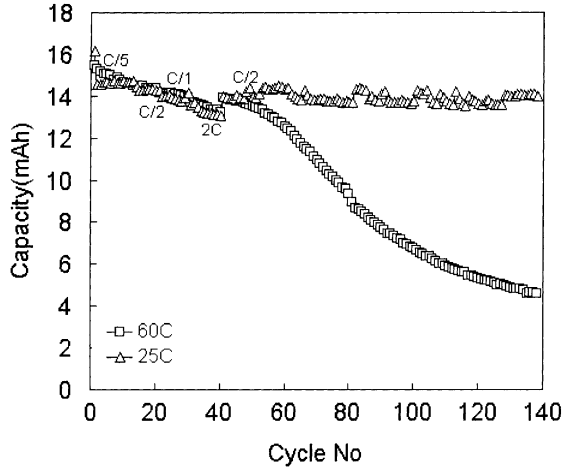

Fig. 2. Cycling performance for pouch cells at 25 and 60 °C. Electrode area 12 cm^2, cut-off voltage 3.0–4.1 V.

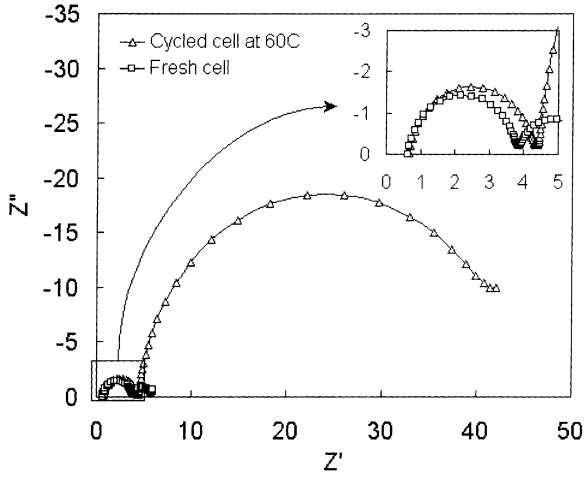

Fig. 4. Nyquist plot for fresh cell and cycled cell at elevated temperature after fully charging. Temperature 25 °C.

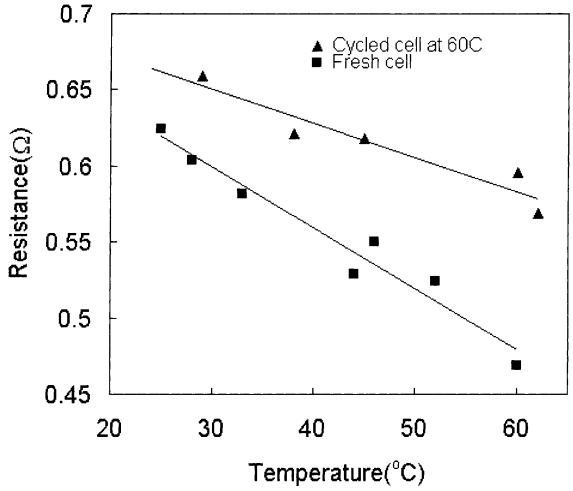

Fig. 5. Electrolyte resistance for fresh cell and cycled cell on temperature.

cathode. However, this assignment of loops has been questioned and further analysis is warranted.

The ohmic portion of the impedance was calculated from the high frequency intercept with the *x*-axis. For all temperatures, the ohmic impedance of the 60 °C-cycled cell was somewhat higher than that of the fresh cell. However, it also shows a significantly weaker dependence on temperature (Fig. 5). Zhang et al. reported that $LiPF_6$ salt is not stable at elevated temperature and is decomposed to PF_5 (g) and LiF (s) [6]. They also observed that electrolyte turned a brown color by the reaction of PF_5 gas and LP40 electrolyte. We also observed a brown stain on the separator after disassembly of cycled cell. They proposed that ionic conductivity of electrolyte decreased due to increasing solvent viscosity and charge carrier loss. Our results are consistent with these findings.

Before disassembly, the 60 °C cell was cooled down and subjected to another *C*/25 "formation" cycle. Fig. 6 shows the calculated differential capacity plot for this test compared to one carried out on the fresh cell. The fresh cell

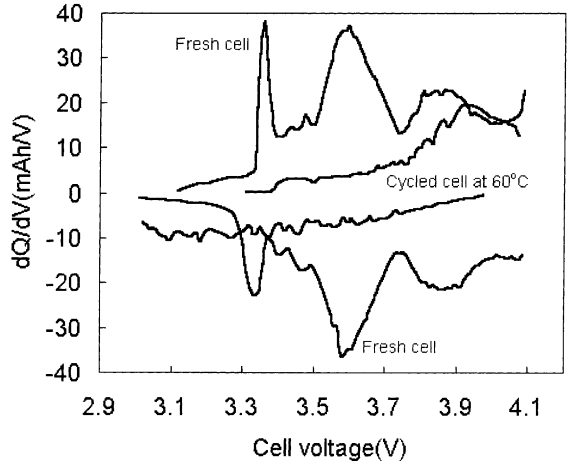

Fig. 6. Comparison of voltage profiles to fresh cell and cycled cell at 60 °C. Temperature 25 °C, *C*/25 rate (0.5 mA).

shows the many, highly reversible peaks for the Li intercalation/deintercalation into graphite and doped $LiNiO_2$ [14]. The plot for the 60 °C-cycled cell shows very different shape compared to fresh cell. Every peak for charging has disappeared except for broad peak at 3.9 V and only a broad peak for discharging is evident at low potential. This plot suggests that the total capacity of the cell has also dropped significantly, in addition to the increase in cell impedance.

There are many reasons for capacity fading in lithium battery [6]. During cycling, the fatigue of crystal structure for active materials and the decomposition of electrolyte including solvent and salt will be accelerated at higher temperatures. Large increases in the cell impedance reduce capacity by causing the cell to reach cut-off voltages earlier. Aging at elevated temperature will result in capacity fade [15]. Recent results from the ATD program suggest that the capacity of cells with this chemistry is reasonably stable to aging at elevated temperature [16]. Simple aging at 45 °C lead to increases in cell impedance on the order of 30%. However, at the *C*/25 rate, even double this rate of impedance rise would not lead to a 65% capacity loss.

Impedance changes with cycling were not measured directly in this study. However, after each half-cycle at *C*/2 the cell was allowed to rest for 15 min. Some indication of the impedance changes with cycling can be obtained by examining the voltage profiles during these rest periods at different points in the cycling. A qualitative separation between the purely ohmic and concentration polarization contributions to the impedance at the end of charge (EOC) and end of discharge (EOD) can be gleaned by comparing the initial voltage drop with the voltage relaxation before the beginning of the succeeding half cycle. These resistances/polarization contributions are illustrated for the 100% SOC in Fig. 7. The measured values for *C*/2 cycles 17, 81 and 139 are summarized in Table 1. It is clear that the concentration

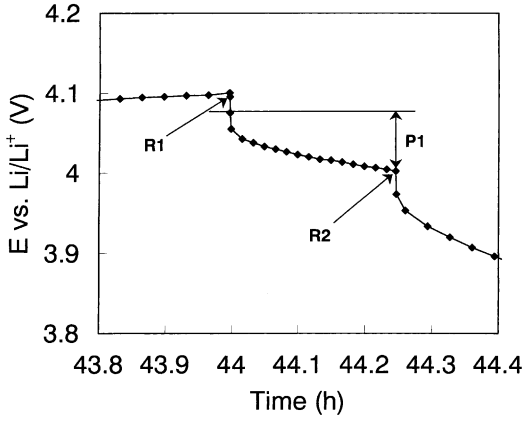

Fig. 7. Location of polarization and ohmic resistance estimates for the end-of-charge data. *R*1 (*R*3) occurs when the current is turned off; *P*1 (*P*2) occurs during the 15 min rest period and *R*2 (*R*4) occurs when the discharge current is turned on. Comparable assignments are made at EOD: *R*3, *P*2 and *R*4.

Table 1
Summary of area-specific resistance values from C/2 cycling of cell at 60 °C

Cycle no. (*C*/2)	End of charge values (Ω cm^2)			End of discharge values (Ω cm^2)		
	*R*1	*R*2	*P*1	*R*3	*R*4	*P*2
17	89	72	3.7	92	92	25
81	174	80	59	224	110	504
139	300	144	154	214	112	744
Change (%) (17–139)	238	100	4030	131	21	2850

polarization or relaxation value is changing the most during cell cycling at 60 °C. This analysis cannot identify the location of the problem. However, it is consistent with an increased diffusion resistance, through an SEI layer, for example. For more insight, various diagnostic techniques were carried out.

3.2. Electrochemical analysis of cell components

To further understand the mechanism of capacity fading in this cell, pieces cut from the disassembled 60 °C pouch cell were studied against fresh lithium with fresh electrolyte, as discussed earlier. The electrodes were charged and discharged at slow rate (*C*/25) between the same voltage limits. However, a shorting problem prevented the 60 °C cell from being completely discharged. Figs. 8 and 9 show the voltage profiles from the abused electrodes compared with those measured with pieces of fresh anode and cathode, respectively. While the cycled anode showed a capacity loss of 10% when compared to a fresh anode, the potential profiles for charging and discharging are almost same to for the two anodes pieces. Previous studies of anode pieces recovered from cycled 18650's showed large film impedance that was removed by continuous cycling and reduction in fresh electrolyte [6]. This behavior was not observed here, probably because any degradation films left on the anode was removed altogether by washing before assembling into the cell with lithium. The results in Fig. 8 suggest that the anode is not a major contributor to capacity loss in the lithium-ion cell at 60 °C.

In contrast to the anode result, Fig. 9 shows the *C*/25 charge and discharge profiles for a washed cathode sample cycled against Li with fresh electrolyte at 25 °C. The lithium removed on charge corresponds to about 30% of the original capacity, suggesting that the cathode was at about 70% SOC as removed from the cell. This is consistent with a loss of lithium inventory from the cell, as has often been cited as a failure mechanism in Li-ion cells. However, the capacity of the sample was not recovered on discharge against fresh Li. On continued cycling, it is clear that only 30% of the original capacity; about the same loss as shown for the full cell in Fig. 2, is available even with fresh Li in the cell. This suggests that the capacity fading of the pouch cell at high temperature stems primarily from some degradation of the cathode. It also confirms that the capacity loss in the cell is not due solely to a loss of lithium inventory. Cobalt doped $LiNiO_2$ is very stable at elevated temperature compared to pure $LiNiO_2$, $LiCoO_2$ and $LiMn_2O_4$. Arai et al. reported that $LiNi_{0.9}M_{0.1}O_2$ (M=Co, Mn, Ti) showed higher reversibility at 40 °C than non-doped $LiNiO_2$ [17]. $LiMn_2O_4$ and $LiCoO_2$

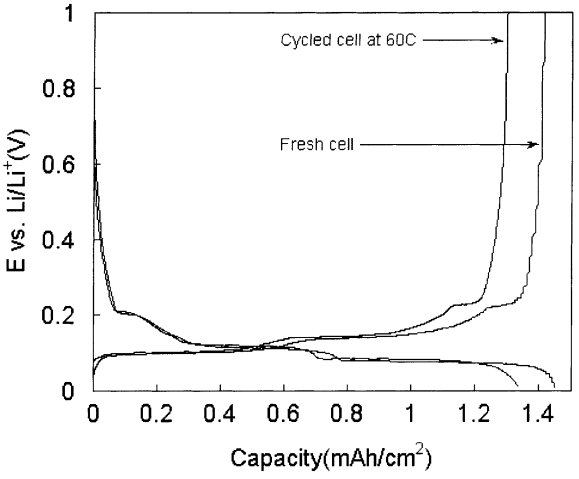

Fig. 8. Charge and discharge profiles for anode cycled at 60 °C for 140 cycles. Temperature 25 °C, electrode area 1 cm, current density 0.05 mA/cm^2 (*C*/25), voltage range 1.0–0.01 V vs. Li/Li$^+$.

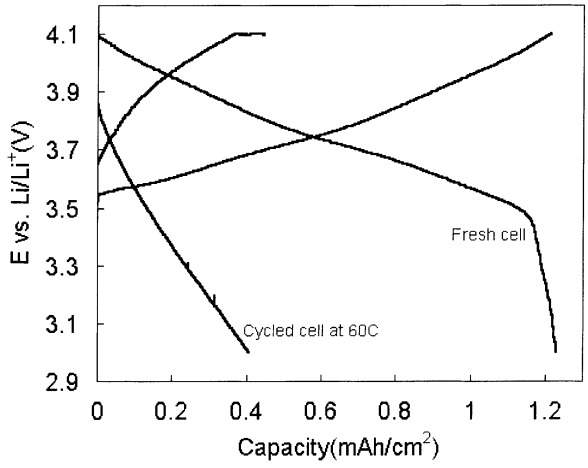

Fig. 9. Charge and discharge profiles for cathode cycled at 60 °C for 140 cycles. Temperature 25 °C, electrode area 1 cm^2, current density 0.05 mA/cm^2 (*C*/25), voltage range 3.0–4.1 V vs. Li/Li$^+$.

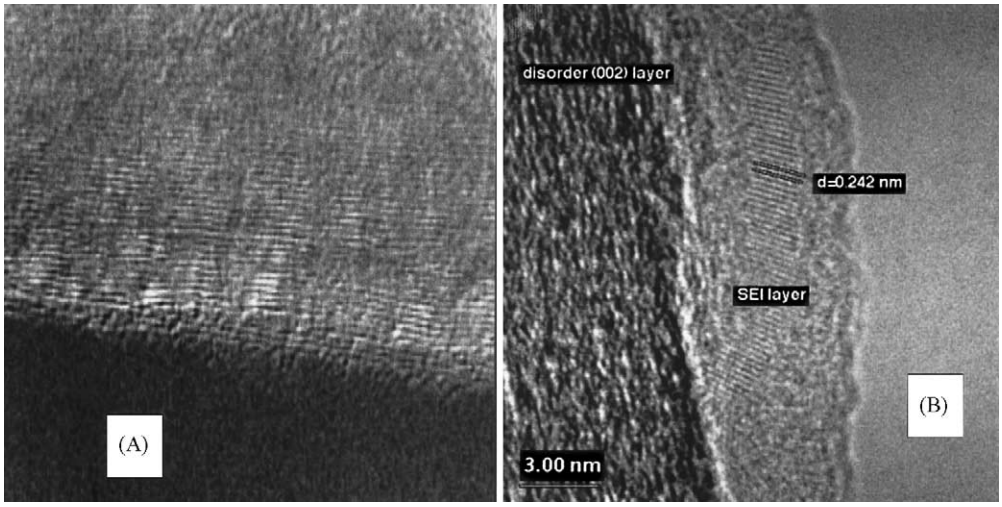

Fig. 10. (A) Mag-10 carbon TEM image, raw material before any exposure to the electrolyte. (B) Mag-10 carbon particle surface after cycling 140 time at 60 °C in $LiPF_6$/EC/DEC electrolyte.

showed severe capacity fading at elevated temperature (50 °C) due to the dissolution of Mn from $LiMn_2O_4$ by HF which was the product for reaction of $LiPF_6$ and water, and micro cracks of $LiCoO_2$ particles by phase transformation between hexagonal and monoclinic phases. However, $LiNi_{0.85}Co_{0.15}O_2$ showed better capacity retention at 50 °C, although there was still some fatigue of crystal structure [18,19]. Cycling at 100% DOD at 60 °C is more severe than that previously reported for this material. However, other possible degradation mechanisms include loss of electronic conductivity in the cathode by physical changes such as the fracture of particle, segregation between active particle and carbon black, swelling of binder, etc. Further diagnostic analysis should help distinguish between the possible degradation modes.

3.3. Anode diagnostics

The electrochemical diagnostics seem to clearly point to the cathode as the source of the capacity fade in the high-temperature cell. However, the anode could also be undergoing changes. TEM analysis of a fresh Mag-10 graphite and a piece of the anode that had been cycled at 60 °C are compared in Fig. 10. The SEI layer is clearly observed in this picture and the lattice fringes match well with Li_2CO_3 (Fig. 10B). The fractured nature of this layer and the thickness is consistent with an SEI that is continually forming, degrading and reforming. In addition, a significant disorder of the originally, very ordered Mag-10 graphite can also be seen in Fig. 10A. However, there is no evidence of this disorder in the electrochemical analysis, shown in the comparison of the dQ/dV plots for the fresh and cycled anode in Fig. 11. Changes in the crystallinity of the graphite electrode with cycling as analyzed with Raman spectroscopy will be discussed in a later publication.

3.4. Cathode diagnostics

X-ray diffraction patterns of cathodes removed from the cycled cells in the discharged state showed no evidence for degradation of the active material or accumulation of new solid phases (Fig. 12). It has been shown [20] that the cell parameters of $Li_xNi_{0.8}Co_{0.2}O_2$ vary in an approximately linear fashion with lithium content, x. Using the measured cell constants for $LiNi_{0.8}Co_{0.15}Al_{0.05}O_2$ and $Li_{0.5}Ni_{0.8}Co_{0.15}Al_{0.05}O_2$ and assuming a similar linear dependence, the lithium content of each cathode was estimated (Fig. 13).

The calculations show that the cell cycled at 25 °C and fully discharged was at an SOC of about 14%. This result is consistent with previous findings for discharged cells. In a fresh cell, the impedance is the highest for a fully discharged

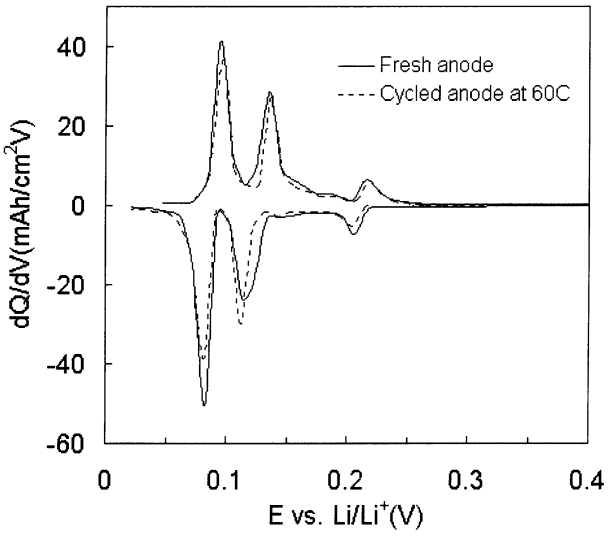

Fig. 11. dQ/dV representation of C/25 test on the anode harvested for a cell cycled at 60 °C over 100% DOD.

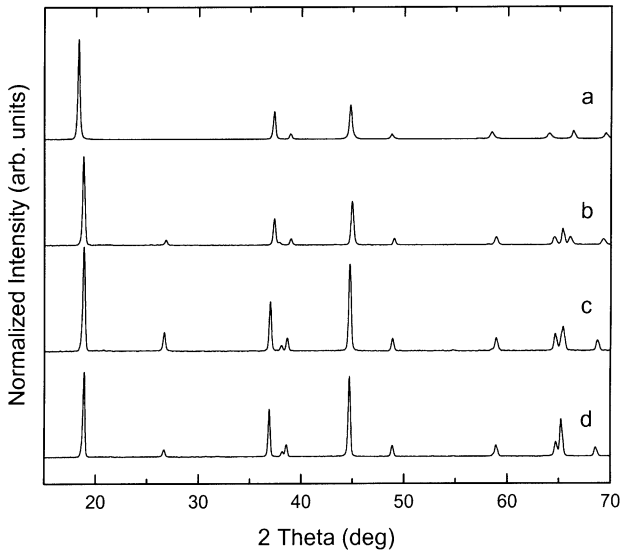

Fig. 12. XRD patterns for (a) uncycled, (b) 25°-cycled, (c) 60 °C-cycled cathodes and (d) $Li_{0.5}Ni_{0.8}Co_{0.15}Al_{0.05}O_2$ powder.

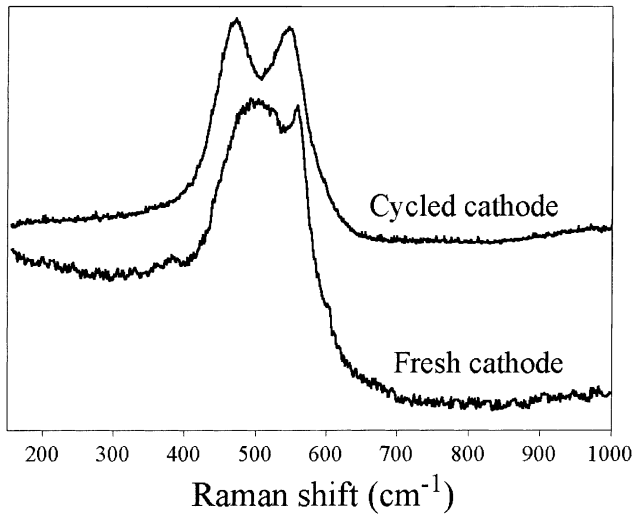

Fig. 14. Raman Spectra for fresh and cycled $LiNi_{0.8}Co_{0.15}Al_{0.05}O_2$ cathodes.

cell. Therefore, a fully discharged cell is only obtained with the use of a taper discharge, which was not used in this work. The cell cycled at 60 °C was at a state of charge of about 56%. This was less completely discharged as noted earlier, due to disconnection problems.

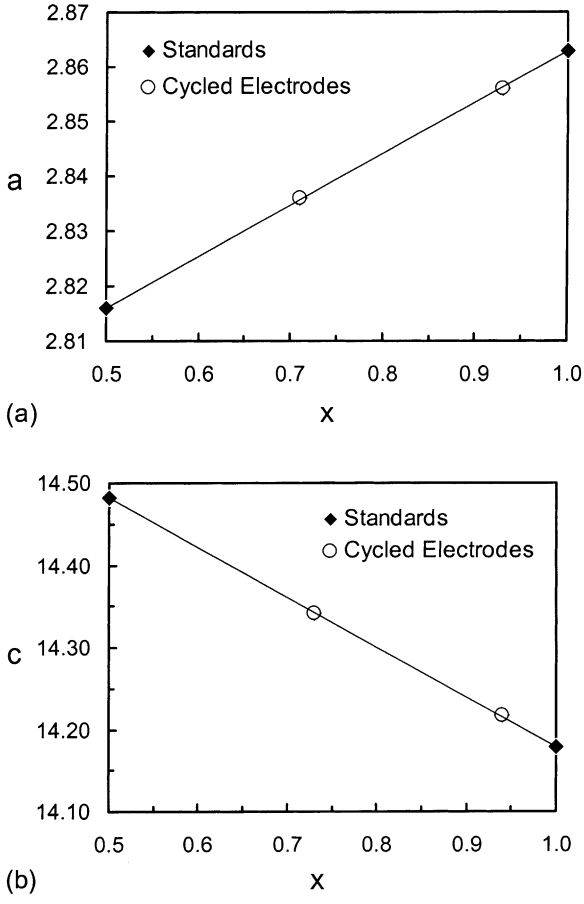

Fig. 13. Lattice parameters (a) a_o and (b) c_o for $Li_xNi_{0.8}Co_{0.15}Al_{0.05}O_2$ standards and cycled cathodes.

The partially-charged nature of the cathode was confirmed with Raman microscopy, as seen in Fig. 14. Cathode surface of the 60 °C-cycled cell consists of almost fully charged $Li_{1-x}Ni_{0.8}Co_{0.15}Al_{0.05}O_2$ particles. The degree of lithiation of individual particles varied slightly between different locations, however, no fully discharged material could be found at the surface of the cathode. Raman spectroscopy is also useful for detecting organic films. However, the presence of carbon in the structure precluded such analysis of these electrodes.

The topography of the cathode cycled at 60 °C (Fig. 15A and C) was essentially very similar to that observed in the room temperature cell and the fresh cathode. The nanocrystalline deposits observed previously in of $LiNi_{0.8}Co_{0.2}O_2$ cathodes [6] were not detected here. This could possibly be due to the stabilising effect of Al additive on the structure of the $Li_{1-x}Ni_{0.8}Co_{0.15}Al_{0.05}O_2$ or less structural damage incurred by the cathodes in this study because they were not calendered before assembly into the cell. It could also be due to the more consistent charge and discharge (no pulse) currents used in this study, though previous results were observed with purely aged electrodes.

However, the CSAFM measurements (Fig. 15B and D) show clearly that surface electronic conductance of the composite cathode changed significantly upon cycling in the tested cell [21]. The images in the right panel represent current response to 1.0 V voltage bias between the sample and the conducting AFM tip, the darker the color of the conductance image the better electronic conductivity of the cathode. Taking into account, all size of the AFM tip, the conductance images reflect local surface conductance rather than bulk properties of the electrode. Cycling at 60 °C (Fig. 15D) led to a dramatic loss of surface electronic

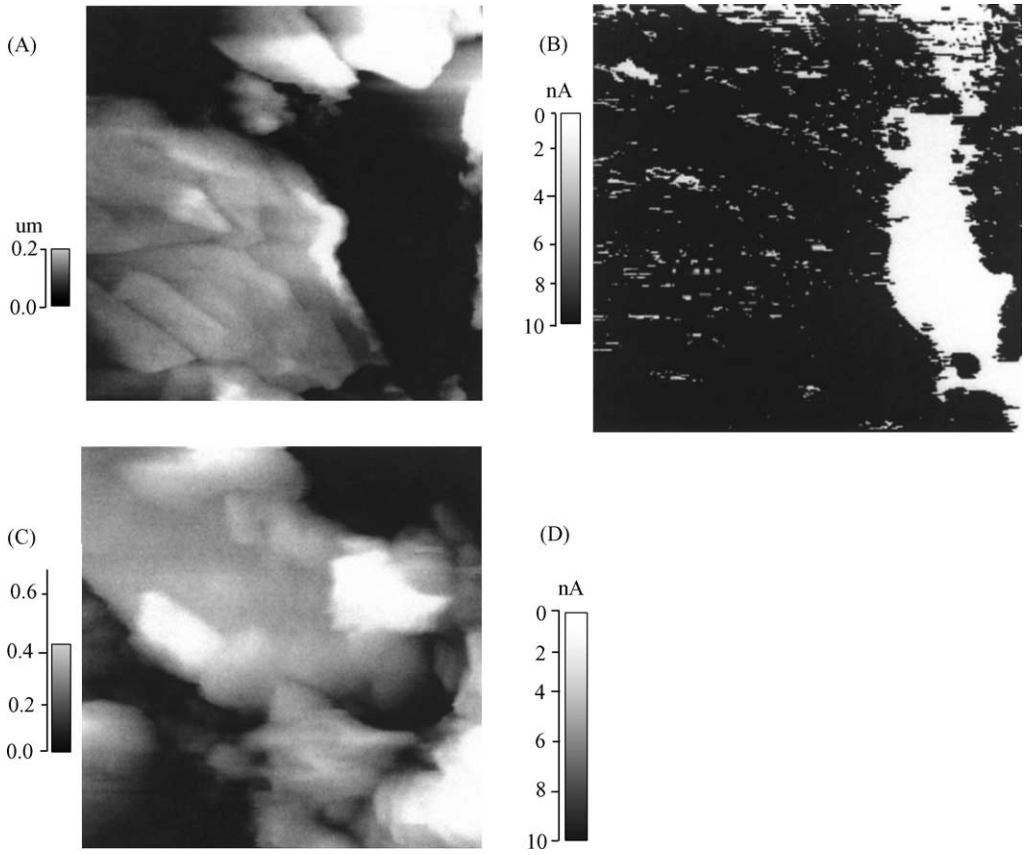

Fig. 15. CSAFM images of fresh (A and B) and 60 °C-cycled (C and D) cathode. The topography is shown on the left (A and C) and the conductivity map of the surface is shown on the right (B and D).

Table 2
Summary of area-specific resistance values from C/25 cycling of a fresh cathode and a piece of the cathode cycled at 60 °C

Cycle 2 (*C*/25)	End of charge values (Ω cm^2)			End of discharge values (Ω cm^2)		
	*R*1	*R*2	*P*1	*R*3	*R*4	*P*2
Fresh cell	60	82	90	380	350	7900
60 °C-cycled	448	553	4140	560	486	9900
Difference (%)	650	570	4500	47	39	25

conductivity. The entire surface of the composite $Li_{1-x}Ni_{0.8}Co_{0.15}Al_{0.05}O_2$ cathode became electronically insulating.

An analysis of the voltage relaxation in the half cells, as carried out for the full cells earlier, is summarized in Table 2 for data from Fig. 9. The impedance is seen to increase greatly for the fully charged cathode. The ohmic portion increases by a factor of 6 while that of the concentration polarization by a factor of 45! The appearance of this high concentration polarization at the end of charge suggests the presence of an SEJ layer with a lithium-ion conductivity that is a strong function of lithium content. When the lithium content drops to a given value, the layer essentially shuts the cell down from further charging. On recharge, the increased lithium content leads to a normally active SEI layer. The increases in the ohmic portion of the resistance with high temperature cycling are present at both the EOC and EOD. These are consistent with a loss of carbon from the structure. Electronic disconnection of cathode active material is ruled out because the active material is clearly homogeneous, as discussed earlier from the XRD results.

4. Conclusions

Pouch cells with graphite and Co- and Al- doped $LiNiO_2$ were cycled at 100% DOD at 25 and 60 °C. Although cycling capacity at 25 °C was essentially constant, about 65% of the initial capacity was lost after 140 cycles at 60 °C. It was observed that the interfacial resistance at cathode increased greatly by impedance analysis. Ohmic resistance

in the full pouch cell also increased, probably due to increasing solvent viscosity and carbon loss from the surface of the cathode. Results for half cell diagnostics of the cycled electrodes showed that the anode did not loose much capacity. However, the capacity of the cathode significantly decreased after cycling at 60 °C. XRD, Raman, and CSAFM analyses of the cell components as well as a careful analysis of voltage profiles during cycling suggest that the source of capacity loss as well as impedance rise in the cathode is due to a low-conductivity SEI layer forming on the cathode. This layer was not directly observed with either Raman spectroscopy or XRD and is probably organic in nature.

References

[1] Q. Wu, W. Lu, J. Prakash, J. Power Sources 88 (2000) 237.
[2] A.N. Jansen, A.J. Kahaian, K.D. Kepler, P.A. Nelson, K. Amine, D.W. Dees, D.R. Vissers, M.M. Thackeray, J. Power Sources 81/82 (1999) 902.
[3] G. Nagasubramanian, R.G. Jungst, D.H. Doughty, J. Power Sources 83 (1999) 193.
[4] J.P. Feller, G.J. Loeber, S.S. Sandhu, J. Power Sources 81/82 (1999) 867.
[5] Y.-E. Hyung, S.-I. Moon, D.-H. Yum, S.-K. Yun, J. Power Sources 81/82 (1999) 842.
[6] X. Zhang, P.N. Ross Jr, R. Kostecki, F. Kong, S. Sloop, J.B. Kerr, K.A. Striebel, E.J. Cairns, F. McLarnon, J Electrochem. Soc. 148 (2001) A463.
[7] PNGV Battery Test Manual, DOE/ID-10597, Revision 3, February 2001.
[8] Batteries for Advanced Transportation Technologies (BATT) Program for Electrochemical Energy Storage, Annual Report, 2000, p. 3.
[9] R.A. Sutula, et al., in: Proceedings of the FY 2000 Progress Report for the Advanced Technology Development Program, US DOE, OAAT, December 2000.
[10] D. Aurbach, A. Zaban, Y. Ein-Eli, I. Weissman, O. Chusid, B. Markovsky, M. Levi, E. Levi, A. Schechter, E. Granot, J. Power Sources 68 (1997) 91.
[11] D. Aurbach, B. Markovsky, I. Weissman, E. Levi, Y. Ein-Eli, Electrochim. Acta 45 (1999) 67.
[12] K.A. Striebel, J. Shim, Performance and Degradation Evaluation of Five Different Commercial Lithium-Ion Cells, LBNL-50500, Berkeley, CA, June 2002.
[13] G. Nagasubramanian, J. Power Sources 87 (2000) 226.
[14] J. Barler, R. Koksbang, M. Yazdi Saidi, Solid State Ionics 89 (1996) 25.
[15] M. Broussely, S. Herreyre, P. Biensan, P. Kasztejna, K. Nechev, R.J. Staniewicz, J. Power Sources 97/98 (2001) 13.
[16] C.G. Motloch, T.C. Murphy, Overview of PNGV Battery Development and Test Programs, in: Proceedings of the Advanced Automatic Battery Conference, Las Vegas, NV, February 2002.
[17] H. Arai, M. Tsuda, Y. Sakurai, J. Power Sources 90 (2000) 76.
[18] K. Dokko, S. Horikoshi, T. Itoh, M. Nishizawa, M. Mohamedi, I. Uchida, J. Power Sources 90 (2000) 109.
[19] K. Dokko, M. Nishzawa, S. Horikoshi, T. Itoh, M. Mohamedi, I. Uchida, Electrochem. Solid State Lett. 3 (2000) 125.
[20] A.I. Saadoune, C. Delmas, J. Solid State Chem. 136 (1998) 8.
[21] R. Kostecki, F. McLarnon, Electrochem. Solid State Lett. 5 (2002) A164.